Atomistic molecular dynamics simulation of the temperature and pressure dependences of local and terminal relaxations in *cis*-1,4-polybutadiene

Georgia Tsolou
Institute of Chemical Engineering and High-Temperature Chemical Processes (FORTH-ICE/HT), Patras GR 26504, Greece; Department of Chemical Engineering, University of Patras, Patras GR 26504, Greece; and Interdepartmental Program of Graduate Studies on "Polymer Science and Technology," University of Patras, Patras GR 26504, Greece

Vagelis A. Harmandaris
Institute of Chemical Engineering and High-Temperature Chemical Processes (FORTH-ICE/HT), Patras GR 26504, Greece and Max Planck Institute for Polymer Research, D-55128 Mainz, Germany

Vlasis G. Mavrantzas[a)]
Institute of Chemical Engineering and High-Temperature Chemical Processes (FORTH-ICE/HT), Patras GR 26504, Greece; Department of Chemical Engineering, University of Patras, Patras GR 26504, Greece; and Interdepartmental Program of Graduate Studies on "Polymer Science and Technology," University of Patras, Patras GR 26504, Greece

(Received 13 December 2005; accepted 18 January 2006; published online 28 February 2006)

The dynamics of *cis*-1,4-polybutadiene (*cis*-1,4-PB) over a wide range of temperature and pressure conditions is explored by conducting atomistic molecular dynamics (MD) simulations with a united atom model on a 32-chain C_{128} *cis*-1,4-PB system. The local or segmental dynamics is analyzed in terms of the dipole moment time autocorrelation function (DACF) of the simulated polymer and its temperature and pressure variations, for temperatures as low as 195 K and pressures as high as 3 kbars. By Fourier transforming the DACF, the dielectric spectrum, $\varepsilon^*=\varepsilon'+i\varepsilon''=\varepsilon^*(\omega)$, is computed and the normalized $\varepsilon''/\varepsilon''_{\max}$ vs $\omega/\omega_{\max}$ plot is analyzed on the basis of the time-temperature and time-pressure superposition principles. The relative contribution of thermal energy and volume to the segmental and chain relaxation processes are also calculated and evaluated in terms of the ratio of the activation energy at constant volume to the activation energy at constant pressure, Q_V/Q_P. Additional results for the temperature and pressure dependences of the Rouse times describing terminal relaxation in the two polymers show that, in the regime of the temperature and pressure conditions covered here, segmental and chain relaxations are influenced similarly by the pressure and temperature variations. This is in contrast to what is measured experimentally [see, e.g., G. Floudas and T. Reisinger, J. Chem. Phys. **111**, 5201 (1999); C. M. Roland *et al.*,J. Polym. Sci. Part B, **41**, 3047 (2003)] for other, chemically more complex polymers that pressure has a stronger influence on the dynamics of segmental mode than on the dynamics of the longest normal mode, at least for the regime of temperature and pressure conditions covered in the present MD simulations. © *2006 American Institute of Physics*. [DOI: 10.1063/1.2174003]

I. INTRODUCTION

In a recent article,[1] we have exploited molecular dynamics (MD) simulations to obtain predictions for the structural and equilibrium dynamic properties of model *cis*-1,4-polybutadiene (*cis*-1,4-PB) systems at pressure $P=1$ atm and temperatures T ranging from 430 to 298 K, i.e., above the melting point, T_m, of *cis*-1,4-PB (close to 270 K).[2] The simulations were carried out with the united atom force field introduced by Smith and Paul[3] on the basis of quantum chemistry calculations. MD predictions for the thermodynamic, structural, conformational, and dynamic properties of *cis*-1,4-PB, presented over a wide range of chain lengths (ranging from C_{32} up to C_{400}), were extensively compared to the available experimental data and other simulation studies, thus fully validating the new force field. In the present work, the MD simulations are extended to significantly lower temperatures (down to 195 K) and higher pressures (up to 3 kbars) in order to study temperature, pressure, and density effects on local (segmental) and terminal (chain) *cis*-1,4-PB dynamics. The work is motivated by the recent experimental observations (with techniques such as dielectric spectroscopy and quasielastic neutron scattering) for the influence of hydrostatic pressure on the local dynamics of polymers such as PB, 1,4-poly(isoprene) (PI), poly(propylene glycol) (PPG), poly(2-vinylpyridine) (P2VP), polyisobutelene (PIB),[4–12] and other glass-forming polymers at temperatures close to the glass transition temperature, T_g.[13–16] Frick *et al.*[4,5] and Cailliaux *et al.*,[6] for example, have presented results from incoherent inelastic neutron scattering on protonated 1,4-PB where the pressure was used as the control parameter demonstrating the different relaxation behavior of isochoric data, while Floudas and Reisinger[7] and Mierzwa *et al.*[17] investi-

[a)]Author to whom correspondence should be addressed. Fax: +30-2610-965-223. Electronic mail: vlasis@chemeng.upatras.gr

gated the pressure effects on the segmental and chain relaxations of PI and polylactides by using both dielectric spectroscopy and rheological measurements. The main conclusion was that the segmental relaxation is more sensitive to pressure variations than terminal relaxation, which also agrees with the more recent studies of Roland *et al.*[11] through dielectric measurements on PPG samples at pressures in excess of 1.2 GPa.

Guided by these experimental studies, and in an effort to, (a) predict the dependence of segmental and chain dynamics on pressure and temperature separately or on density, (b) investigate whether the two dependencies are different or not, and (c) compute the relative contributions of volume and thermal energy to the dynamic response, all from first principles, we have extended our recent MD simulation study of *cis*-1,4-PB to significantly lower temperature and higher pressure conditions than previously addressed, using a C_{120} *cis*-1,4-PB model as a test system. Since details on the force-field parameterization are reported in Ref. 1, these will not be repeated here; thus, the work presented in this paper is organized as follows. Section II discusses the molecular characteristics of the simulated polymer, and the temperature and pressure conditions at which the simulations were carried out. Section III reports the predictions of the atomistic MD simulations for (a) the time decay of the DACF of the simulated *cis*-1,4-PB system as a function of temperature and pressure (Sec. III A), (b) the dielectric loss spectrum and its shift with temperature and pressure in scaled coordinates (Sec. III B), and (c) the relative contributions of thermal energy and density to segmental dynamics (Sec. III C). Section IV is concerned with issues of terminal relaxation in the system and how chain relaxation compares to the segmental dynamics under isobaric or isothermal conditions. The paper concludes with Sec. V discussing the major findings of the present work and future plans.

II. SIMULATION DETAILS

The model used in the *cis*-1,4-PB simulations is the same with that employed in our recent work on the study of static and dynamic properties of the same polymer in the melt state ($T \geqslant 298$ K) at $P=1$ atm.[1] It is a united atom model in which every CH_n group in the chain is represented as a single interaction site (see Fig. 1), based on the descriptions proposed by Gee and Boyd[18] and Smith and Paul[3] from quantum chemistry calculations. With this united atom model, a strictly monodisperse 32-chain *cis*-1,4-PB system with 128 carbon atoms per chain (herein referred to as the C_{128} *cis*-1,4-PB system) was simulated in this paper in the isothermal-isobaric (*NPT*) statistical ensemble, at temperatures ranging from 430 to 195 K and pressures from 1 atm to 3 kbars (see Table I).

Initial configurations for the two simulated systems were created using CERIUS2 software[19] followed by a minimization procedure.[20] These were subsequently subjected to an exhaustive preequilibration run via a long *NVT* MD simulation at $P=1$ atm and at a density value equal to the experimentally measured one at $T=413$ K, followed by a long *NPT* MD production run at the same conditions for about 50 ns.

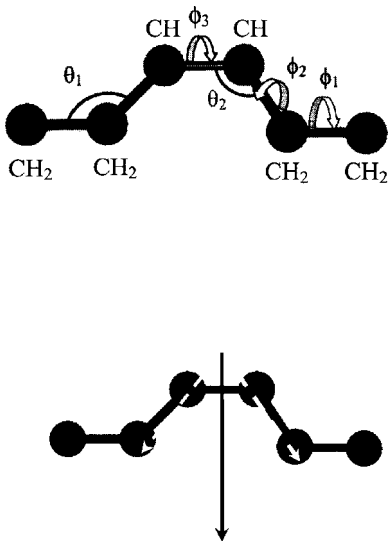

FIG. 1. United atom model for the structural unit of *cis*-1,4-PB (a) and the vector **M** of its dipole moment (b).

Subsequent MD simulations at progressively lower temperatures were started from the equilibrated configurations obtained at the end of the MD simulations at a higher temperature. Similarly, fully equilibrated configurations obtained from long MD runs at low pressures were used as initial configurations for the MD runs at the higher pressures. The equations of motion were integrated by using a multiple-time step algorithm [the reversible reference system propagator algorithm (rRESPA)[21] method], with the small integration step selected equal to 1 fs and the large one equal to 5 fs, in all MD runs. The duration of the MD production runs varied from 50 ns for the higher temperatures and lower pressures up to 1 μs for the lower temperatures and higher pressures. All MD runs were carried out with the large-scale atomic/molecular massively parallel simulator (LAMMPS) code[22] that can run on any parallel platform supporting the MPI library.

To also simulate the *cis*-1,4-PB system under isochoric conditions, the temperature and pressure conditions were carefully chosen so as to correspond (in many cases) to the same density for the simulated system. This was achieved by trial-and-error MD runs, and the (T,P) pairs located are listed in Table II. For comparison, we mention that the experimentally accepted glass transition temperatures at $P=1$ atm are between 160 and 175 K for infinitely long *cis*-1,4-PB.[2,23]

TABLE I. Temperature and pressure conditions at which the C_{128} *cis*-1,4-PB system has been simulated.

T (K)	P (kbar)
195	1.013×10^{-3}
225	1.013×10^{-3}
270	1.013×10^{-3},0.5,1.0,2.5
310	1.013×10^{-3},1.5,2.5
343	1.013×10^{-3},1.0,1.5,2.0,2.5
380	1.013×10^{-3},1.0,1.5,2.0,2.5,3.0
413	1.013×10^{-3},1.0,1.5,2.0,2.5,3.0
430	1.013×10^{-3},1.0,1.5,2.0,2.5,3.0

TABLE II. Different temperature and pressure pairs corresponding to the same density for the simulated C_{128} *cis*-1,4-PB system.

Density (g/cm^3)	T (K)	P (kbar)
0.94±0.01	270	1.013×10^{-3}
	413	1.5
0.97±0.01	225	1.013×10^{-3}
	270	0.5
	343	1.5
	380	2
	430	2.5
0.98±0.01	310	1.5
	343	2
	380	2.5
	430	3.0

III. SEGMENTAL RELAXATION

The local or segmental relaxations in the simulated *cis*-1,4-PB system were evaluated in terms of the time decay of its DACF, and its dependence on temperature and pressure separately, or density.

A. Dipole moment time autocorrelation function

The monomer of *cis*-1,4-PB bears a component of the dipole moment vector **M** perpendicular to the chain-backbone (see Fig. 1), therefore segmental dynamics in *cis*-1,4-PB can be studied by dielectric spectroscopy.[24] What is measured in the dielectric experiments[25–27] is the complex dielectric permittivity defined as

$$\varepsilon^* = \varepsilon' + i\varepsilon'', \tag{1}$$

where ε' and ε'' denote the real and imaginary parts of the permittivity, which are measured as a function of frequency, ω, temperature, T, and more recently pressure, P. The characteristic dielectric relaxation time is then obtained by analyzing (fitting) the experimental data with an empirical equation, such as the Havriliak and Negami equation.[28] The complex dielectric permittivity is an experimental observable which can also be extracted from the MD simulation data for the time autocorrelation function of the system dipole moment through the following relation of linear response theory:[26]

$$\frac{\varepsilon' + i\varepsilon''}{\Delta\varepsilon} = 1 - i\omega\int_0^\infty \Phi(t)\exp(-i\omega t)dt. \tag{2}$$

In Eq. (2), $\Phi(t)$ is the dipole moment autocorrelation function defined as

$$\Phi(t) = \frac{\langle \mathbf{M}(t)\cdot\mathbf{M}(0)\rangle}{\langle \mathbf{M}(0)^2\rangle} \tag{3}$$

and $\Delta\varepsilon$ the dielectric strength, given by

$$\Delta\varepsilon = \frac{4\pi\langle \mathbf{M}^2\rangle}{3Vk_BT}. \tag{4}$$

The dipole moment vector $\mathbf{M}(t)$ that appears in Eq. (3) is the single-chain dipole moment calculated as the sum of all monomer dipole moment vectors along a chain at time t, with brackets $\langle\cdots\rangle$ representing ensemble averages over all chains in a system volume V. This happens because the ensemble average in the DACF is dominated by the self-(a chain with itself) time correlations; in contrast, contributions from cross correlations (a chain with a different chain) expressing the collective character of dipole relaxation are unimportant,[29] something which was also verified in the present MD study. By assigning a dipole moment vector to each monomer of *cis*-1,4-PB, the time evolution of the DACF can be tracked in the course of the MD simulation and then used in Eqs. (2)–(4) to extract $\varepsilon''=\varepsilon''(\omega)$.

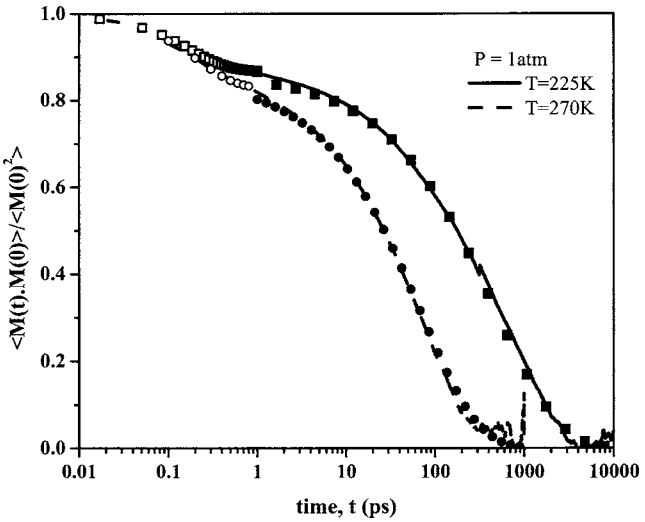

FIG. 2. Time autocorrelation function of the dipole moment, $\Phi(t)$, at different temperatures along an isobar as obtained from the present MD simulations with the C_{128} *cis*-1,4-PB system, in log-linear coordinates. The symbols represent the best fittings to the simulation data according to the piecewise continuous function of Eq. (5) of the main text.

In Fig. 2, $\Phi(t)$, as predicted from our MD simulations, is plotted (continuous lines) as a function of time in log-linear coordinates along the different isothermal paths. Similar to the behavior of the torsional time autocorrelation functions of the ϕ_1 and ϕ_2 dihedrals along the *cis*-1,4-PB chain,[1] $\Phi(t)$ exhibits a rapid decay at times less than 1 ps (primitive or noncooperative relaxation), followed by a rather slow decorrelation at later times, which was in all cases (even at the lowest temperatures and highest pressures studied) accessible by our MD simulation. All curves, and especially the higher temperature ones, show the same structure. One sees a short-time hump, followed by a quasilinear region leading into the long-time α relaxation.[30] The bend between the two regions occurs at about 1 ps for all temperatures, suggesting that the bond angle vibrations and torsional librations inducing a fast reorientational motion on the dipoles (and not activated transitions) are responsible for the hump. A closeup of the decay of $\Phi(t)$ with t in Fig. 3 confirms that the time scale of the hump is independent of the temperature.

The experimental evidence[31] for the nearly exponential decay of $\Phi(t)$ at subpicosecond time scales (or, equivalently, for the existence of a crossover at time t_c between 1 and 2 ps) comes from a number of measurements, including, for example, quasielastic neutron-scattering measurements on poly(vinylchloride) (PCV),[32–34] high-frequency dielectric

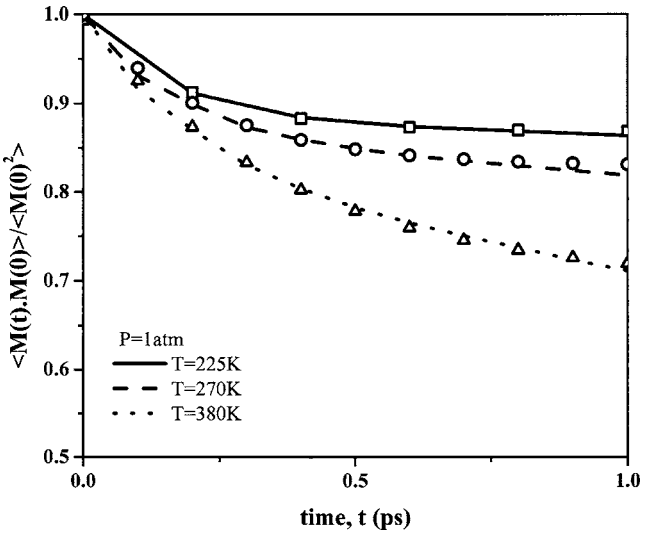

FIG. 3. Same as with Fig. 2 but in linear coordinates and for times up to 1 ps to emphasize that the time scale of the short-time behavior (primitive dynamics) is independent of temperature. The symbols represent the best fittings to the simulation data according to the piecewise continuous function of Eq. (5) of the main text.

measurements on glassy and nonglassy ionic conductors,[35] etc., performed at temperatures well above T_g where the primitive relaxation time becomes short (on the order of 10 ps or less). In the context of the coupling model,[31,36] t_c marks the onset of chaos (the passage from noncooperative to cooperative dynamics) caused by the anharmonic (nonlinear) nature of the interactions between the basic molecular units (e.g., monomers in polymers or small molecules in glass-forming van der Waals liquids customarily modeled as Lennard-Jones fluids); therefore, its value should be insensitive to temperature variations.

In calculations involving Fourier transforming $\Phi(t)$ with respect to t to obtain the dielectric relaxation spectrum, it is often convenient to describe the time dependence of $\Phi(t)$ via analytical expressions. Based on the above observations for the two different (the rapid at short and the slow at long time scales) modes of decay, computed $\Phi(t)$ curves can be fit quite accurately piecewise by two analytical expressions. The first is a fast-decaying exponential describing the initial decorrelation at times up to $t_c=1$ ps, and the second a slowly decaying stretched exponential or Kohlrausch-Williams-Watts (KWW) function capturing the decay of $\Phi(t)$ beyond $t_c=1$ ps,

$$\Phi(t)=\begin{cases} 1+A_1\left[\exp\left(-\dfrac{t}{\tau_0}\right)-1\right], & t<t_c \\ A_2\exp\left(-\dfrac{t-t_c}{\tau^d_{\mathrm{kww}}}\right)^{\beta^d}, & t>t_c \end{cases}. \tag{5}$$

In Eq. (5), τ_0 is the characteristic relaxation time in the subpicosecond regime, $A_2=1+A_1[\exp(-t_c/\tau_0)-1]$, and τ^d_{kww} and β^d the characteristic relaxation time and the stretching exponent parameters of the KWW function fitting the DACF; the corresponding (total) correlation time, τ^d_c, is obtained from the integral of $\Phi(t)$ from $t=0$ up to $t=\infty$:

$$\tau^d_c=\int_0^\infty \Phi(t)dt. \tag{6}$$

As shown in Figs. 2 and 3, the modified exponential function $\Phi(t)=1+A_1[\exp(-t/\tau_0)-1]$ fits (open symbols) the dynamics in the region $t<t_c(\approx 1$ ps) almost perfectly, that is the true short-time decay of the computed curve is not exponential but superexponential. The corresponding primitive or noncooperative relaxation time τ_p is then easily found as the integral of this function from $t=0$ up to $t=t_c$: $\tau_p=(1-A_1)t_c+A_1\tau_0[1-\exp(-t_c/\tau_0)]$. Also accurate are the fits (filled symbols) in the longer-time region, $t>t_c(\approx 1$ ps), with the KWW function (see Fig. 2). The primitive relaxation time τ_p was found to change only infinitesimally with temperature and pressure. At $P=1$ atm, for example, its value increased from 0.76 to 0.90 ps as the temperature was decreased from 430 down to 225 K, or from 0.84 to 0.85 ps as the pressure was raised from 1 atm to 2.5 kbars (keeping T constant, equal to 310 K).

Best-fit values for β^d for all the studied temperature and pressure conditions are summarized in Table III. Values of β^d characterizing the stretched exponential decay of the DACF in *cis*-1,4-PB for times beyond 1 ps are found to vary between 0.60 and 0.82 in the temperature range of 195–430 K (for $P=1$ atm). They are also observed to decrease somewhat as the pressure is raised.

TABLE III. Numerical values of the stretching exponent β^d of the KWW function employed to fit the MD predictions for the time decay of the DACF at long time scales (beyond 1 ps) in the simulated C_{128} *cis*-1,4-PB system, as a function of temperature and pressure [see Eq. (5) in main text].

	β^d							
P (kbar)	T (K)							
	195	225	270	310	343	380	413	430
1.013×10^{-3}	0.60±0.03	0.62±0.03	0.67±0.03	0.70±0.02	0.74±0.02	0.73±0.01	0.80±0.01	0.82±0.01
0.5	⋯		0.66±.02	⋯	⋯	⋯	⋯	⋯
1	⋯		0.65±.02	⋯	⋯	0.73±0.03	0.79±0.03	0.81±0.03
1.5	⋯		⋯	0.69±0.03	0.72±0.03	⋯	0.79±0.03	0.81±0.03
2	⋯		⋯	⋯	0.70±0.03	0.72±0.03	0.77±0.03	0.80±0.03
2.5	⋯		⋯	0.68±0.03	⋯	0.72±0.03		⋯
3	⋯		⋯	⋯	⋯	0.70±0.03	0.76±0.03	0.79±0.03

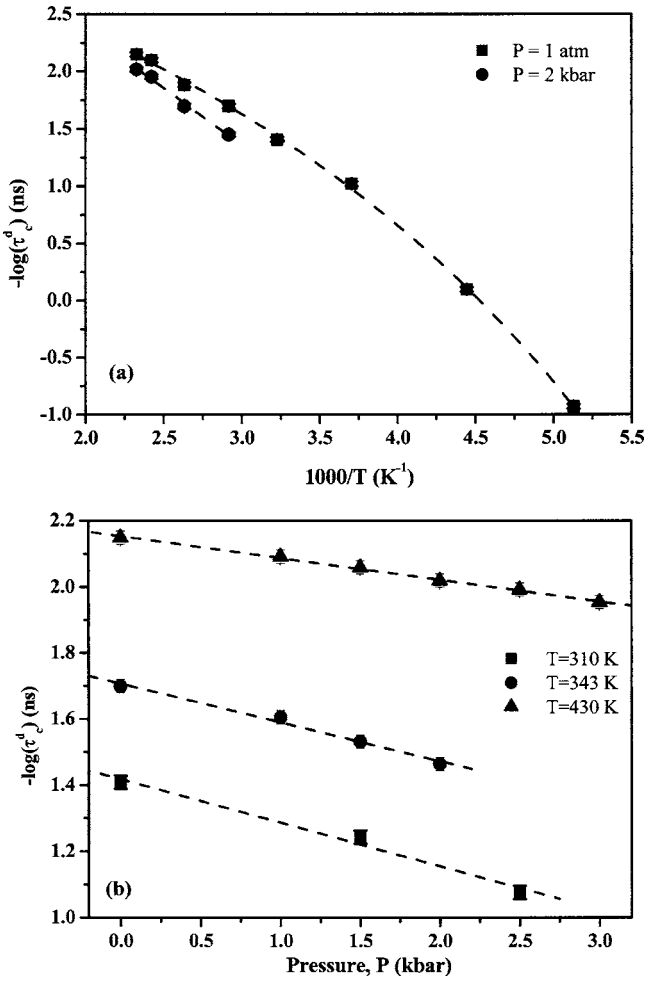

FIG. 4. (a) Temperature dependence of the relaxation times, τ_c^d, as obtained from the present MD simulations with the C_{128} *cis*-1,4-PB along two different isobars. Dashed lines denote the best fits to the simulation data with a VFT function. (b) Pressure dependence of the relaxation times, τ_c^d, as obtained from the present MD simulations with the C_{128} *cis*-1,4-PB at three different isotherms in a log-linear plot. Dashed lines represent the best linear fits to the simulation data.

The curve representing the time decay of the DACF was always found to lie between the curves representing the time decay of the torsional autocorrelation functions (TACFs) for the ϕ_1 and ϕ_2 dihedrals along a *cis*-1,4-PB chain (results not shown here), indicating that $\Phi(t)$ describes the relaxation of a *cis*-1,4-PB segment extending at most two adjacent monomers along the chain. In general, the total correlation times estimated either from the torsional or the dipole moment time autocorrelation functions exhibit the same temperature and pressure dependences. In Figs. 4(a) and 4(b) the correlation time τ_c^d describing the time decay of the DACF is plotted as a function of temperature along the isobar, or as a function of pressure along an isotherm. Figure 4(a) shows that the temperature dependence of τ_c^d can be captured quite well by a modified Vogel-Fulcher-Tammann (VFT) function[9,37] of the form;

$$\tau_c^d = \tau_0^d \exp\left(\frac{D^d T}{T - T_0^d}\right), \tag{7}$$

where D^d is a dimensionless parameter and T_0^d the "ideal" glass transition temperature or the Vogel temperature. The values providing the best VFT fits to the MD simulation data are $\log(\tau_0^d/\text{ns}) = (7.3 \pm 0.2)$, $D^d = -(4 \pm 1)$, and $T_0^d = (100 \pm 5)$ K.

TABLE IV. Computed values of activation volume, ΔV^d, and their temperature dependence for the simulated *cis*-1,4-PB system. Superscript *d* is used to emphasize activation volumes calculated from relaxation times computed on the basis of the time decay of the dipole moment time autocorrelation function (DACF).

T(K)	270	310	380	430
ΔV^d(cm^3/mol)	14.2	7.8	6.5	5.4

Figure 4(b), on the other hand, shows that τ_c^d increases exponentially with increasing pressure. From the best-fit slopes of the $-\log(\tau_c^d)$ vs P plots, values of the activation volume ΔV^d associated with *cis*-1,4-PB local dynamics can be determined, through $\Delta V^d = 2.303RT(\partial \log \tau_c^d / \partial P)_T$; these are reported in Table IV and are found to increase with decreasing temperature: ΔV^d increases from (5.4 ± 0.2) cm^3 mol^{-1} at $T = 430$ K to (14.2 ± 0.2) cm^3 mol^{-1} at $T = 270$ K. According to Papadopoulos *et al.*,[9] dielectric spectroscopy (DS) measurements on P2VP have shown that the activation volume for the α relaxation slightly above T_g is very high, but falls rapidly with increasing temperature approaching the monomer volume at $T \sim T_g + 70$ K. Similar results have been obtained by Floudas *et al.*[38] for *cis*-1,4-PI. For *cis*-1,4-PB, the values of ΔV^d extracted from our MD simulation data are consistent with (although slightly smaller than) the time-resolved optical microscopy measurements of Kirpatch and Adolf[10] on different molecular weight *cis*-1,4-PB samples, according to which the activated volume varies between 19 and 35 cm^3 mol^{-1} in the temperature range of 323–303 K.

It is also interesting to mention that if one neglects the primitive or noncooperative subpicosecond relaxation regime in the DACF [see Eq. (5)] and fits the *entire* $\Phi(t)$ vs t curve with a KWW function (this is usually what the experimentalists do, since the regime of the noncooperative relaxation is not easily accessible), then the computed best-fit β^d values show a stronger pressure dependence than those reported here on the basis of Eq. (5); as a consequence, the computed ΔV^d values are larger and hence closer to the experimentally measured ones.

B. Dielectric spectrum

A direct comparison of our MD simulation predictions against experimental data for segmental dynamics in *cis*-1,4-PB can be performed at the level of the normalized dielectric loss spectrum, $\varepsilon''/\Delta\varepsilon$, which is the experimental observable in DS. $\varepsilon''/\Delta\varepsilon$ has been calculated here by Fourier transforming [see Eq. (2)] the piecewise analytical representation of $\Phi(t)$ [Eq. (5)] with respect to t allowing us to obtain $\varepsilon''/\Delta\varepsilon$ over the range of frequencies ω between 10^7 and 10^{12} s^{-1}. For even higher frequencies ($\omega \geqslant 10^{12}$ s^{-1}, short-time period: $t \leqslant t_c = 1$ ps), such a calculation, unfortunately, is not possible due to the numerical inaccuracies associated with the Fourier transform. To overcome this, the method employed by Doxastakis *et al.*[39] and Saiz *et al.*[40] was em-

ployed, based on the analytical expressions proposed by Williams *et al.*[41] for approximating the KWW function for low,

$$\frac{\varepsilon^*(\omega)-\varepsilon_\infty}{\varepsilon_0-\varepsilon_\infty}=\sum_{n=1}^{\infty}(-1)^{n-1}\frac{(\omega\tau_{\mathrm{KWW}})^{n-1}}{\Gamma(n)}\Gamma\left(\frac{n+\beta-1}{\beta}\right)\times\left[\cos\left(\frac{(n-1)\pi}{2}\right)+i\sin\left(\frac{(n-1)\pi}{2}\right)\right] \quad (8a)$$

and high $[-1\leqslant\log(\omega\tau_{\mathrm{KWW}})\leqslant-4$ when $\beta>0.25]$,

$$\frac{\varepsilon^*(\omega)-\varepsilon_\infty}{\varepsilon_0-\varepsilon_\infty}=\sum_{n=1}^{\infty}\frac{(-1)^{n-1}}{(\omega\tau_{\mathrm{KWW}})^{n\beta}}\frac{\Gamma(n\beta+1)}{\Gamma(n+1)}\times\left[\cos\left(\frac{n\beta\pi}{2}\right)-i\sin\left(\frac{n\beta\pi}{2}\right)\right] \quad (8b)$$

frequencies. Computed $\varepsilon''/\Delta\varepsilon$ spectra over a wide range of frequencies, ω, are shown under various isobaric and isothermal conditions in parts (a) and (b) of Fig. 5. In their common frequency range, the high-frequency results for $\varepsilon''/\Delta\varepsilon$ calculated by means of Eq. (8b) (symbols) and through a direct application of Eq. (2) (solid line) are compared in part (c) of Fig. 5, and for all practical purposes coincide.

The curves shown in Fig. 5(a) present a single peak characteristic of the α-relaxation process, which shifts to lower frequencies (longer times) with decreasing temperature. In an analogous manner, as the pressure is raised to high values, the relaxation of the dielectric spectra slows down [see Fig. 5(b)]. The shape of curves reported in Fig. 5 is in excellent qualitative agreement with measured DS spectra for a variety of 1,4-PB samples,[42,43] indicating that the MD simulation captures the time scales of segmental motion almost accurately. However, due to the differences in microstructure (the simulations use 100% *cis*-1,4-PB while the experiments are carried out on PB samples containing in general totally different *cis-trans*-vinyl contents), it is not possible to carry out a strict quantitative comparison between experimental data and the simulation predictions of the present study.

Figures 6 and 7 show the temperature and pressure dependences of the position of the peak, $\omega_{\max}$, in the dielectric spectrum. $\omega_{\max}$ is seen to decrease with decreasing temperature (keeping pressure constant) or with increasing pressure (keeping temperature constant). For example, its value drops from 1.7×10^{11} to 1.2×10^{8} s^{-1} when T is decreased from 430 to 195 K (keeping P constant, equal to 1 atm), or from 7.8×10^{10} to 4.6×10^{10} s^{-1} when P is raised from 1 atm to 3 kbars (keeping T constant, equal to 380 K). For comparison, experimental data[42,44] and data from previous simulations with a random copolymer of 1,4-PB (Ref. 45) have been included within Fig. 6. In general, for the same temperature and pressure conditions, the present MD simulations predict somewhat higher $\omega_{\max}$ values than those of the literature, which is attributed to the different microstructure of the experimental samples or of the simulated PB system (containing a significant portion of *trans*-1,4 and 1,2-vinyl units). Computed $\omega_{\max}$ values are observed to follow a different dependence with temperature than with pressure. The temperature dependence, in the range of 195–430 K studied here, obeys the Vogel-Fulcher (VF) function,

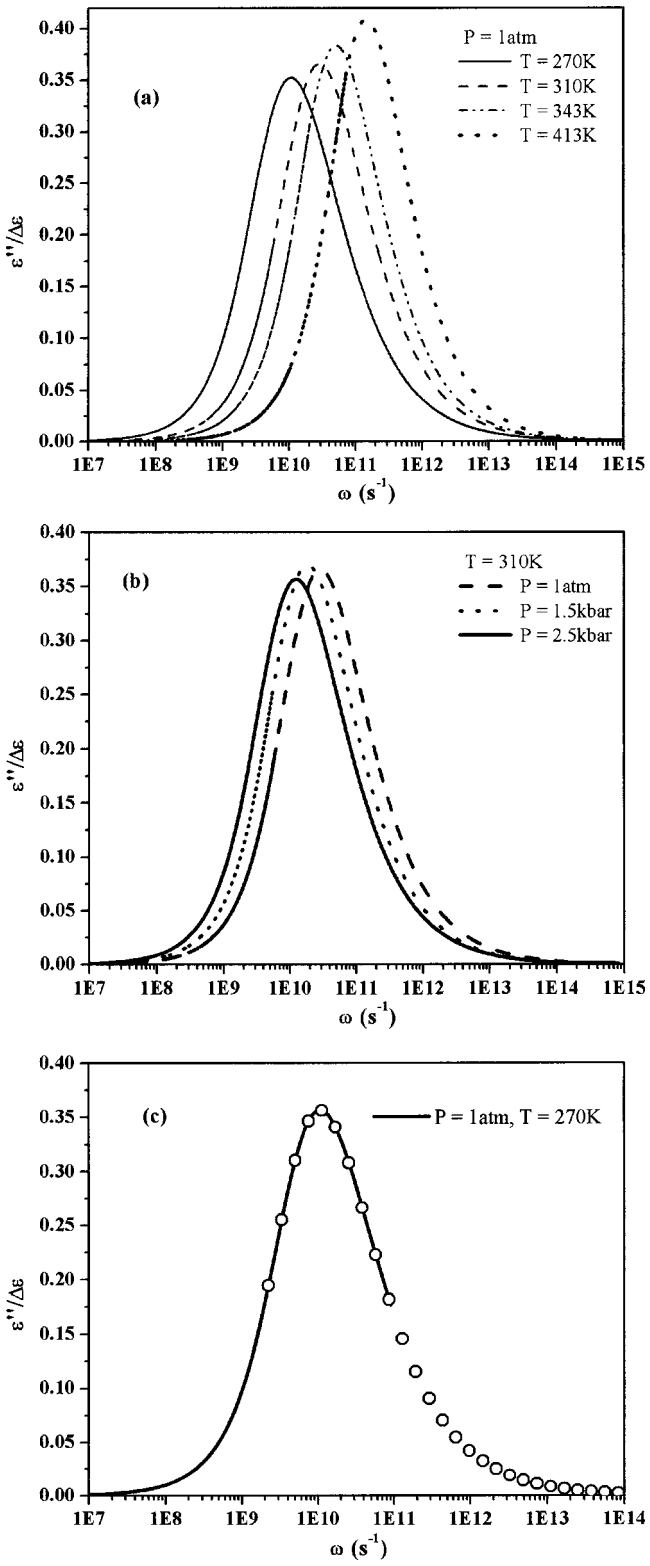

FIG. 5. Predicted dielectric loss spectrum and its variation with: (a) temperature (at $P=1$ atm), and (b) pressure (at $T=310$ K). Included in part (c) of the figure (symbols) is the part of the spectrum computed on the basis of Eq. (8b) referring to high frequencies.

$$\log\omega_{\max}=\log\omega_0+\frac{B}{T-T_0}, \quad (9)$$

with the best-fit values of the parameters as follows: $\log(\omega_0/\mathrm{Hz})=(12.5\pm0.5)$, $B=-(433\pm2)$ K, $T_0=(97\pm1)$ K.

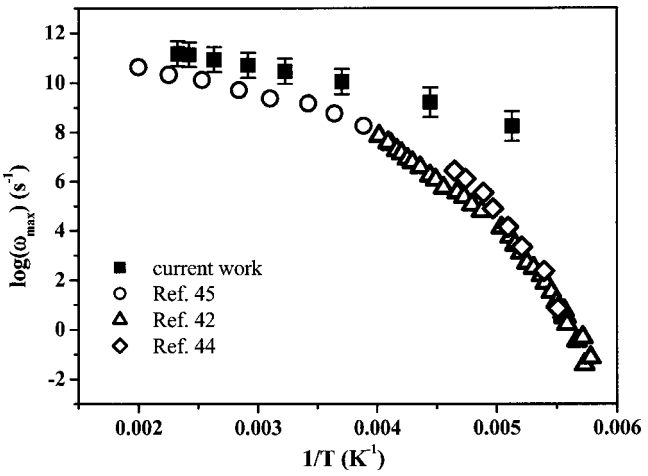

FIG. 6. MD-based predictions for the dielectric loss frequency at the maximum of the spectrum, ω_{max}, plotted against inverse temperature, at $P=1$ atm.

The pressure dependence of ω_{max}, on the other hand, is described in accordance with the variation of the DACF relaxation times with P under isothermal conditions, that is through a linear function of $\log(\omega_{max})$ with P. To the best of our knowledge, there exist no experimental data available in the literature for the pressure dependence of ω_{max} for PB with which we could compare the predictions of the present MD study.

In order to test the validity of the time-temperature and time-pressure superposition principles, the computed dielectric loss spectra from the present MD simulations are shown in Figs. 8 and 9 in the form of $\varepsilon''/\varepsilon''_{max}$ vs ω/ω_{max} plots, through small vertical and horizontal shifts that bring their peaks on top of each other. By observing then whether the normalized $\varepsilon''/\varepsilon''_{max}$ vs ω/ω_{max} curves superimpose or not, we can pronounce on the validity of the two superposition principles. According to Fig. 8, all scaled curves corresponding to temperatures between 430 and 270 K do superimpose, demonstrating the validity of the time-temperature superposition principle for 100% *cis*-1,4-PB in this temperature range. However, as the temperature is lowered below 270 K

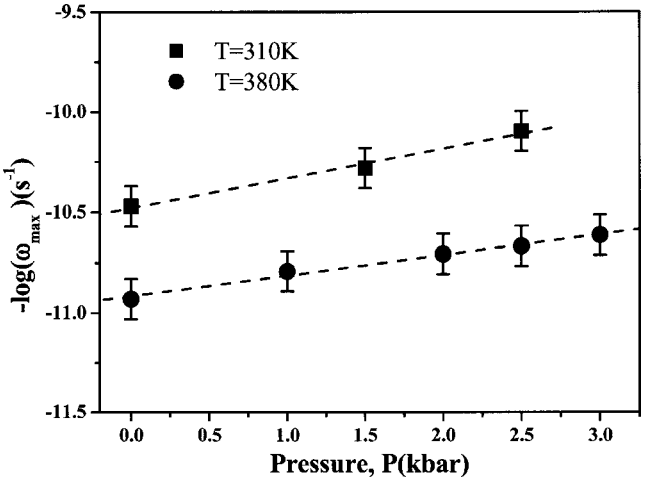

FIG. 7. MD-based predictions for the pressure dependence of the dielectric loss frequency at the maximum, ω_{max}, at $T=310$ K and $T=380$ K.

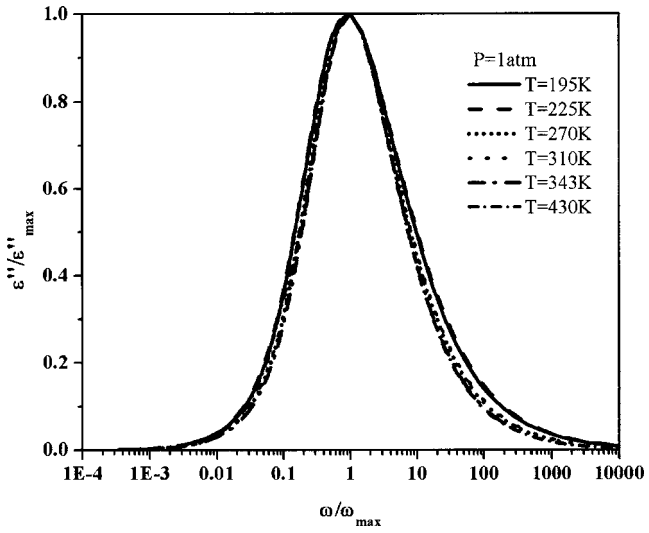

FIG. 8. Normalized dielectric loss data, as obtained from the present MD simulations with the C_{128} *cis*-1,4-PB system, plotted against normalized frequency at different temperatures ($P=1$ atm).

(e.g., down to $T=225$ or 195 K in Fig. 8), the obtained $\varepsilon''/\varepsilon''_{max}$ vs ω/ω_{max} curves are seen to somewhat widen (i.e., to open up) both from below (low frequencies) and above (higher frequencies); such a behavior indicates a deviation from the time-temperature superposition principle as T is lowered below 225 K, signaling the emergence of additional relaxation mechanisms beyond the primary or α relaxation. Although in the literature there is a strong experimental evidence that 100% *cis*-1,4-PB does not exhibit a β relaxation[46] due to its tight chain packing, a future work will investigate this issue in more detail by extending the present MD simulations for *cis*-1,4-PB at even lower temperatures (within a few degrees of its T_g value).

$\varepsilon''/\varepsilon''_{max}$ vs ω/ω_{max} plots at different pressure conditions (keeping the temperature constant, equal to 310 K) are presented in Fig. 9, demonstrating also the validity of the time-pressure superposition principle (therefore, the absence of

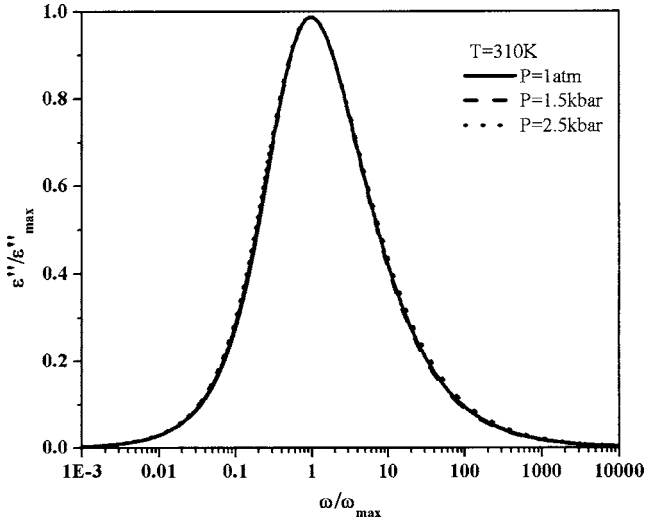

FIG. 9. Normalized dielectric loss data, as obtained from the present MD simulations with the C_{128} *cis*-1,4-PB system, plotted against normalized frequency at different pressures ($T=310$ K).

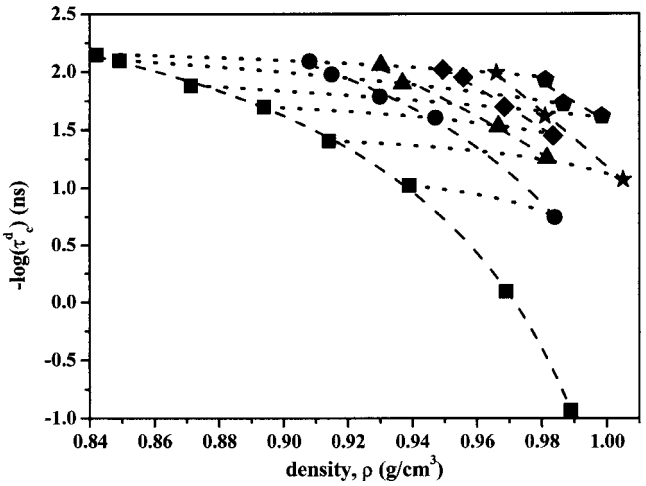

FIG. 10. Predicted relaxation times for the simulated C_{128} *cis*-1,4-PB plotted against density at different temperature and pressure conditions, on a log-linear plot. Dotted and dashed lines represent the best fits to the MD simulation data with a VFT function.

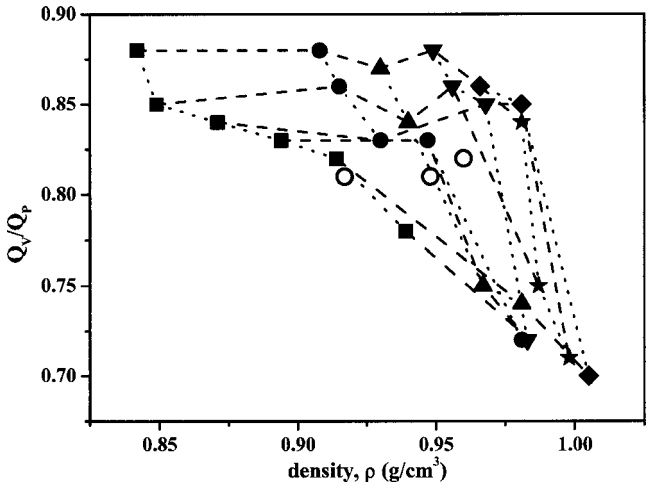

FIG. 11. MD-based predictions for the Q_V/Q_P ratio of the activation energies under constant volume and under constant pressure as a function of density for the C_{128} *cis*-1,4-PB system. Filled symbols indicate Q_V/Q_P values obtained with Eq. (11) and open circles Q_V/Q_P values obtained with Eq. (12).

any additional relaxation mechanisms at high frequencies) over the studied range of pressures (1 atm–3 kbars).

C. Relative contributions of thermal energy and density to segmental relaxation

The study of the combined effect of T and P on segmental relaxation can be used to test the validity of free volume theories and energy landscape models for the dynamics of glass-forming materials. According to the former (free volume theories), segmental relaxation is entirely determined by the available amount of free volume in the system. Given the one-to-one correspondence between the system specific volume and system free volume, free volume theories propose that systems with the same density should essentially follow a similar relaxation process, i.e., there should be no change in their segmental relaxation times under isochoric conditions. To test this hypothesis, torsional or dipole moment autocorrelation times are plotted in Fig. 10 as a function of density to obtain what is known as a "density representation of PVT data."[9] To this end, in Fig. 10, we display plots of $-\log(\tau_c^d)$ as a function of density for the simulated polymer as obtained via different variations in temperature and pressure. We immediately observe then that the local relaxation times at a fixed density are larger at lower temperatures, in full agreement with the experimental measurements of Kirpatch and Adolf.[10] It is also observed that the local relaxation times change more dramatically under isobaric (solid lines) than under isothermal (dashed lines) conditions. Undoubtedly, temperature has a dominant contribution to segmental relaxation compared to pressure.

The density dependence of correlation times displayed in Fig. 10 is described quite accurately with a modified VFT function,

$$\log(\tau_c^d) = \log(\tau_0^\rho) + \left(\frac{D_\rho \rho}{\rho - \rho_0}\right), \tag{10}$$

where D_ρ is a dimensionless parameter and ρ_0 the ideal glass density. Best-fit values for the VFT equation parameters are as follows: $\log(\tau_0^\rho/\text{ns}) = (3.2 \pm 0.2)$, $D_\rho = 0.3 \pm 0.2$ and $\rho_0 = (1.05 \pm 0.05)$ g cm^{-3}, under all studied isobaric conditions.

We have further calculated the ratio Q_V/Q_P of the activation energies under constant density, $Q_V = -RT^2(\partial \ln \tau_c^d/\partial T)_V$, and under constant pressure, $Q_P = -RT^2(\partial \ln \tau_c^d/\partial T)_P$, which takes values between 0 and 1. In fact, the ratio Q_V/Q_P can be calculated directly from the $-\log(\tau_c^d)$ vs ρ plots of Fig. 10 through:[9]

$$\frac{Q_V}{Q_P} = 1 - \frac{(\partial \ln \tau_c^d/\partial \rho)_T}{(\partial \ln \tau_c^d/\partial \rho)_P}. \tag{11}$$

How Q_V/Q_P changes with density, for different T and P conditions in the simulated polymer, is demonstrated in Fig. 11. The lines in the figure are guides for the eye indicating isobaric (the dotted ones) and isothermal (the dashed ones) conditions. Q_V/Q_P values well below 0.5 indicate density as the controlling parameter of local dynamics whereas Q_V/Q_P values above 0.5 indicate the thermal demand associated with activated local motion as the controlling parameter of local dynamics. According to the plots of Fig. 11, for the *cis*-1,4-PB system: (a) the ratio Q_V/Q_P is always larger than 0.5 for all studied densities, revealing the dominant contribution of thermal energy to segmental relaxation. (b) The ratio Q_V/Q_P lies between 0.71 and 0.88, which agrees remarkably well with the time-resolved optical spectroscopy measurements of Kirpatch and Adolf.[10] (c) Temperature has a strong effect on Q_V/Q_P along isobaric curves. (d) The ratio Q_V/Q_P is practically insensitive to pressure variations.

The ratio Q_V/Q_P can also be calculated independently from[9]

$$\frac{Q_V}{Q_P} = 1 - \left(\frac{\partial P}{\partial T}\right)_V \left(\frac{\partial T}{\partial P}\right)_{\tau_c^d}, \tag{12}$$

where $(\partial P/\partial T)_V$ can be extracted from the present simulation data for the PVT properties of the C_{128} *cis*-1,4-PB system and $(\partial T/\partial P)_{\tau_c^d}$ from the data presented in Figs. 4(a) and 4(b).

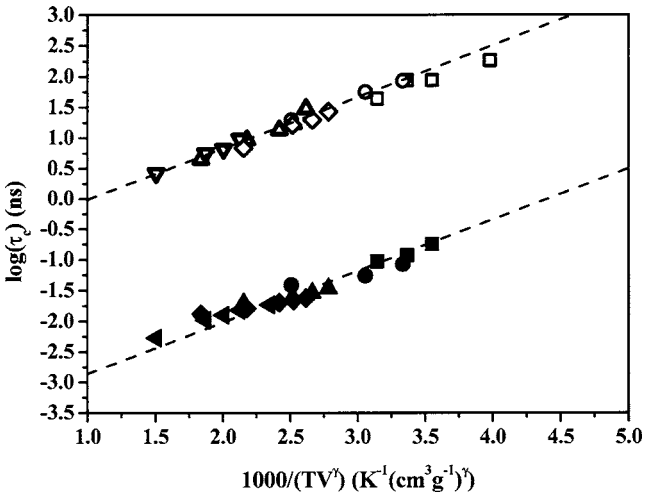

FIG. 12. Predicted relaxation times describing segmental (filled symbols) and chain (open symbols) relaxations, as a function of the combined variable $T^{-1}V^{-\gamma}$, for the C_{128} *cis*-1,4-PB system.

Unfortunately, the narrow interval over which isochoral MD simulation data at different temperature and pressure conditions coincide does not allow us to obtain the full Q_V/Q_P spectrum (i.e., Q_V/Q_P values for all simulated densities). Despite this, however, we managed to reliably calculate Q_V/Q_P with Eq. (12) for three different density points and the results obtained are shown in Fig. 11 with open circles indicating their consistency with the values obtained from Eq. (11).

Quite recently, Casalini and Roland[12,47] proposed a universal scaling of local relaxation times based on the assumption of an inverse power law of the form $\varphi(r) \propto r^{-3\gamma}$ for an effective repulsive potential governing primarily the liquid structure (with the attractive forces playing the role of a background potential), where r denotes the intermolecular separation and γ is a material parameter. With such a scaling, Casalini and Roland[12] and Ngai *et al.*[48] found that the relaxation data for both the segmental and normal modes obtained from dielectric relaxation measurements on PPG and 1,4-PI can be fairly well described as a function of the combined variable $T^{-1}V^{-\gamma}$, and practically superimpose. Guided by this idea, Fig. 12 reports plots (filled symbols) of the segmental relaxation times as a function of the combined variable $T^{-1}V^{-\gamma}$, for the C_{128} *cis*-1,4-PB system. For completeness, also shown in Fig. 12 (open symbols) is the scaling of the chain longest relaxation time for the same system (calculated from the time decay of the chain end-to-end unit vector autocorrelation function, as explained in detail in the next section) with the combined variable $T^{-1}V^{-\gamma}$. All segmental and all chain relaxation times are observed to drop onto the same straight line, with the best fits (dashed lines) to the simulation data being obtained for a value of the scaling exponent γ equal to 2.8 ± 0.2. The values of γ, that more accurately fitted the experimental dielectric relaxation spectra of PPG and 1,4-PI, were 2.5 ± 0.35 and 3.0 ± 0.15, respectively.[12]

IV. GLOBAL (CHAIN) DYNAMICS

The simulation results presented in Sec. III have addressed mainly the aspects of local dynamics in *cis*-1,4-PB. By employing pressure as an additional thermodynamic variable either in atomistic MD simulations or in experiments such as dielectric spectroscopy is very advantageous, since it allows investigating not only how (for example) the segmental α relaxation is split from the more localized β relaxation but also how the local (segmental) and global (chain) relaxations are affected under different thermodynamic conditions. To this end, based on dielectric spectroscopy measurements on a type-*A* polymer (PI), Floudas and Reisinger[7] and Floudas *et al.*[38] have reported that the external pressure exerts a stronger influence on the dynamics of segmental mode than on the dynamics of the longest normal mode, which, consequently, should result in a crossing of the two modes at a high enough applied pressure, higher than 14 kbars.[7,38] Similar conclusions have been drawn by Roland *et al.*[11] Floudas and co-workers[17,38] for other polymers. The dynamics of the segmental mode has also been reported to be more sensitive (compared to that of the normal modes) to temperature changes (keeping pressure constant),[49–52] leading to the crossing of the two relaxation modes at a temperature approximately 10% higher than T_g.

Terminal relaxation in the simulated polymer system can be evaluated through the time decay of the autocorrelation function for the chain end-to-end unit vector, $\langle \mathbf{u}(t)\mathbf{u}(0) \rangle$. Following Ref. 1, by fitting the simulation data with a stretched exponential (or KWW) function, one can calculate the characteristic longest orientational relaxation time, τ_R, describing the decorrelation of the highest normal mode (the Rouse time) in the simulated system. Computed τ_R values are plotted (open symbols) as a function of temperature in Fig. 13(a); for comparison, also included within Fig. 13(a) are the corresponding correlation times, τ_c^d, characterizing segmental relaxation (filled symbols). It is immediately observed that, like segmental relaxation times, chain relaxation times are described quite accurately by a modified VFT equation,

$$\tau_R = \tau_0^R \exp\left(\frac{D^R T}{T - T_0^R}\right), \tag{13}$$

with the best-fit values of the VFT parameters as follows: $\log(\tau_0^R/\text{ns}) = (4.5 \pm 0.2)$, $D^R = -(4.5 \pm 0.2)$, and $T_0^R = (118 \pm 5)$ K. For comparison, we recall from Sec. III A that the corresponding best VFT fits describing segmental relaxation in *cis*-1,4-PB were $\log(\tau_0^d/\text{ns}) = (7.3 \pm 0.2)$, $D^d = -(4 \pm 1)$, and $T_0^d = (100 \pm 5)$ K. Interestingly enough, the segmental and chain relaxation times are influenced equally by temperature variations in the studied temperature range 195–430 K for *cis*-1,4-PB.

The pressure dependence of segmental and chain relaxation times in the simulated polymer is shown in Fig. 13(b). Similarly to the pressure dependence of segmental relaxation times (see Sec. III A above), the logarithm of the chain relaxation times, $-\log(\tau_R)$, is also observed to vary linearly with pressure, with a slope very close to that of the curve describing the pressure dependence of the logarithm of the segmental relaxation time, $-\log(\tau_c^d)$. Like temperature, and in contrast to what is measured experimentally,[7,11,17,38] the pressure is predicted here to exert the same influence on both relaxation modes (segmental and terminal). This can be explained either in terms of the different molecular architecture of the simulated polymer compared to that of the samples on

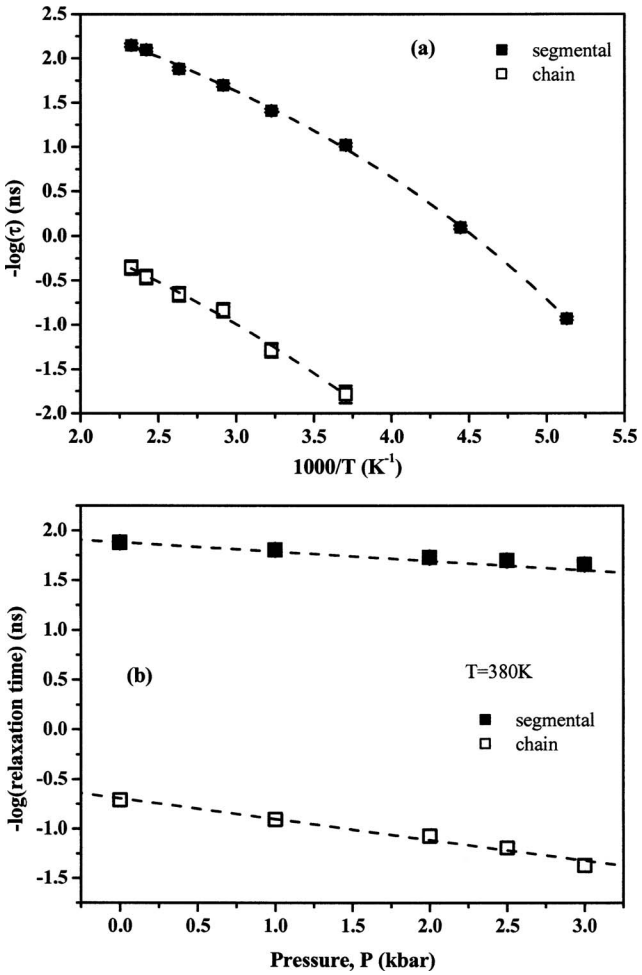

FIG. 13. (a) Relaxation times describing segmental (filled symbols) and chain (open symbols) relaxations in the C_{128} *cis*-1,4-PB as a function of temperature on a log-linear plot ($P=1$ atm). Dashed lines represent the best fits to the MD simulation data with a VFT equation. (b) Relaxation times describing segmental (filled symbols) and chain (open symbols) relaxations in the C_{128} *cis*-1,4-PB system at $T=380$ K as a function of pressure on a log-linear plot. Dashed lines represent the best linear fits to the MD simulation data.

which the experimental studies have been carried out (being mostly type-*A* polymers)[24] or by the fact that the lowest temperature addressed in the present simulation study is several degrees above the glass transition temperature ($T_g=160$ -175 K) (Refs. 2 and 23) of the simulated polymer.

V. CONCLUSIONS

We have presented the results from long atomistic MD simulations of a C_{128} *cis*-1,4-PB system under different temperature and pressure conditions concerning aspects of its segmental and chain relaxation processes, and thoroughly compared them against available experimental data. Computed time autocorrelation functions for the dipole moment are described in terms of two regimes: An initial, short-time regime extending to ca. 1 ps at all temperatures and pressures studied, and a longer-time regime where the relaxation slows down leading to the principal α relaxation of the polymer. The transition between the two regimes is rather sharp. In the subpicosecond regime (also known as primitive or α relaxation in the context of the coupling model), dynamics is close to exponential. Dynamics in the second regime, on the other hand, is well described by a stretched exponential (or KWW) function. The characteristic relaxation times of the two different regimes were computed and analyzed as a function of temperature and pressure.

The MD-based predictions for the total correlation time, τ_c^d, characterizing segmental relaxation in *cis*-1,4-PB at temperatures as low as 195 K and at pressures as high as 3 kbars support a VFT dependence on temperature and an Arrhenius-type of dependence on pressure. Computed values for the activation volume governing segmental relaxation in *cis*-1,4-PB compare quite satisfactorily with reported experimental values from dielectric spectroscopy measurements.

Results have also been reported for the shape of the dielectric loss spectrum of *cis*-1,4-PB, obtained by Fourier transforming the computed DACF with respect to time, under the isothermal and isobaric conditions. The dielectric spectrum exhibits only one peak representative of the α relaxation, whose position shifts towards lower frequencies as the temperature is decreased or as the pressure is increased. A Vogel-Fulcher (VF) equation is observed to describe the temperature dependence of its frequency at the maximum of the spectrum, $\omega_{\max}$; the pressure dependence of $\omega_{\max}$, on the other hand, is captured better with an Arrhenius-type of equation. Normalized $\varepsilon''/\varepsilon''_{\max}$ vs $\omega/\omega_{\max}$ plots have also been analyzed on the basis of the time-temperature and time-pressure superposition principles over the range of temperature (430–195 K) and pressure (1 atm–3 kbars) conditions covered in the present simulations.

The computed values of the ratio Q_V/Q_P, quantifying the relative contribution of thermal energy and volume to segmental relaxation, were always found to be above 0.5, indicating temperature as the controlling thermodynamic variable governing segmental relaxation in *cis*-1,4-PB, and in excellent agreement with the recently reported experimental data based on time-resolved optical spectroscopy.[10]

By carrying out the MD simulations for times on the order of hundreds of nanoseconds (and up to 1 μs, in a few cases), we have also been able to track the dynamics of the slowest normal mode in the simulated polymer. Simulation results for the temperature and pressure dependences of the Rouse times describing terminal relaxation in the polymer show that, in the regime of conditions studied here, segmental and chain relaxations in *cis*-1,4-PB are influenced similarly by pressure and temperature variations.

Future work will address dynamics in *cis*-1,4-PB at even lower temperatures (within a few degrees above and below its T_g value) in order to elucidate the issues related to the origin of glass transition (the arrest of segmental dynamics at low enough temperatures) for this polymer. Analyzing aspects of its segmental relaxation on the basis of the coupling model will also be pursued.

ACKNOWLEDGMENTS

We are grateful to the Greek Secretariat for Research and Technology (GSRT) for financial support in the course of this work through the AKMON Programme (Title: Design of heterogeneous materials for new applications in technologies

of energy and environment, Code No. 61). Very fruitful discussions with Professor George Floudas and Professor Doros Theodorou are greatly appreciated.

[1] G. Tsolou, V. G. Mavrantzas, and D. N. Theodorou, Macromolecules **38**, 1478 (2005).
[2] J. Brandup and E. H. Immergut, *Polymer Handbook*. (Wiley, New York, 1989).
[3] G. D. Smith and W. Paul, J. Phys. Chem. A **102**, 1200 (1998).
[4] B. Frick, G. Dosseh, A. Cailliaux, and C. Alba-Simionesco, Chem. Phys. **292**, 311 (2003).
[5] B. Frick, C. Alba-Simionesco, K. H. Andersen, and L. Willner, Phys. Rev. E **67**, 051801 (2003).
[6] A. Cailliaux, C. Alba-Simionesco, B. Frick, L. Willner, and I. Goncharenko, Phys. Rev. E **67**, 010802 (2003).
[7] G. Floudas and T. Reisinger, J. Chem. Phys. **111**, 5201 (1999).
[8] M. Mierzwa, G. Floudas, M. Neidhofer, R. Graf, H. W. Spiess, W. H. Meyer, and G. Wegner, J. Chem. Phys. **117**, 6289 (2002).
[9] P. Papadopoulos, D. Peristeraki, G. Floudas, G. Koutalas, and N. Hadjichristidis, Macromolecules **37**, 8116 (2004).
[10] A. Kirpatch and D. B. Adolf, Macromolecules **37**, 1576 (2004).
[11] C. M. Roland, R. Casalini, T. Psurek, S. Pawlus, and M. Paluch, J. Polym. Sci., Part B: Polym. Phys. **41**, 3047 (2003).
[12] R. Casalini and C. M. Roland, Colloid Polym. Sci. **283**, 107 (2004).
[13] B. Frick and D. Richter, Science **267**, 1939 (1995).
[14] K. L. Ngai, in *Physical Properties of Polymers*, edited by J. Mark, K. L. Ngai, W. Graessley, L. Mandelkern, E. Samulski, J. Koenig, and G. Wignall, (Cambridge University Press, Cambridge, 2004), pp. 72.
[15] A. Kisliuk, Y. Ding, J. Hwang, J. S. Lee, B. K. Annis, M. D. Foster, and A. P. Sokolov, J. Polym. Sci., Part B: Polym. Phys. **40**, 2431 (2002).
[16] K. Binder and W. Kob, *Glassy Materials and Disorder Solids: An Introduction to Their Statistical Mechanics* (World Scientific, Singapore, 2005).
[17] M. Mierzwa, G. Floudas, J. Dorgan, D. Knauss, and J. Wegner, J. Non-Cryst. Solids **307**, 296 (2002).
[18] R. H. Gee and R. H. Boyd, J. Chem. Phys. **101**, 8028 (1994).
[19] www.accelrys.com/cerius2/
[20] D. N. Theodorou and U. W. Suter, Macromolecules **18**, 1467 (1985).
[21] G. J. Martyna, M. E. Tuckerman, D. J. Tobias, and M. L. Klein, Mol. Phys. **87**, 1117 (1996).
[22] S. Plimpton, J. Comput. Phys. **117**, 1 (1995).
[23] J. E. Mark, *Polymer Data Handbook*. (Oxford University Press, New York, 1999).
[24] W. H. Stockmayer, Pure Appl. Chem. **15**, 539 (1967).
[25] A. K. Jonscher, *Dielectric Relaxation in Solids* (Chelsea, London, 1983).
[26] G. Williams, Chem. Rev. (Washington, D.C.) **72**, 55 (1972).
[27] H. Watanabe, Macromol. Rapid Commun. **22**, 127 (2001).
[28] S. Havriliak and S. Negami, Polymer **8**, 161 (1967).
[29] D. A. McQuarrie, *Statistical Mechanics* (HarperCollins, New York, 1976).
[30] O. Ahumada, D. N. Theodorou, A. Triolo, V. Arrighi, C. Karatasos, and J. P. Ryckaert, Macromolecules **35**, 7110 (2002).
[31] K. L. Ngai, J. Phys.: Condens. Matter **11**, A119 (1999).
[32] J. Colmenero, A. Arbe, and A. Alegria, Phys. Rev. Lett. **71**, 2603 (1993).
[33] K. L. Ngai, J. Colmenero, A. Alegria, and A. Arbe, Macromolecules **25**, 6727 (1992).
[34] R. A. Zorn, J. Colmenero, B. Frick, D. Richter, and U. Buchenau, Phys. Rev. E **52**, 781 (1995).
[35] K. L. Ngai, J. Non-Cryst. Solids **203**, 232 (1996).
[36] K. L. Ngai, J. Phys.: Condens. Matter **12**, 6437 (2000).
[37] K. Mpoukouvalas and G. Floudas, Phys. Rev. E **68**, 031801 (2003); K. Mpoukouvalas, G. Floudas, S. H. Zhang, and J. Runt, Macromolecules **38**, 552 (2005).
[38] G. Floudas, C. Gravalides, T. Reisinger, and G. Wegner, J. Chem. Phys. **111**, 9847 (1999).
[39] M. Doxastakis, D. N. Theodorou, G. Fytas, F. Kremer, R. Faller, F. Muller-Plathe, and N. Hadjichristidis, J. Chem. Phys. **119**, 6883 (2003).
[40] E. Saiz, E. Riande, and R. Diaz Calleja, J. Phys. Chem. A **101**, 7324 (1997).
[41] G. Williams, D. C. Watts, S. B. Dev, and A. M. North, Trans. Faraday Soc. **67**, 1323 (1971).
[42] A. Arbe, D. Richter, J. Colmenero, and B. Farago, Phys. Rev. E **54**, 3853 (1996).
[43] C. G. Robertson and C. M. Roland, Macromolecules **33**, 1262 (2000); R. D. Deegan and S. R. Nagel, Phys. Rev. B **52**, 5653 (1995).
[44] A. Aouadi, M. J. Lebon, C. Dreyfus, B. Strube, W. Steffen, A. Patkowski, and R. M. Pick, J. Phys.: Condens. Matter **9**, 3803 (1997).
[45] G. D. Smith, O. Borodin, and W. Paul, J. Chem. Phys. **117**, 10350 (2002).
[46] R. P. Gupta, J. Phys. Chem. **66**, 1 (1962); J. Mathew, M. Shen, and T. F. Schatzki, J. Appl. Polym. Sci. **23**, 299 (1979); R. J. Morgan, L. E. Nielsen, and R. Buchdahl, J. Appl. Phys. **42**, 4653 (1971).
[47] R. Casalini and C. M. Roland, Phys. Rev. E **69**, 062501 (2004); R. Casalini and C. M. Roland, Phys. Rev. B **71**, 014210 (2005).
[48] K. L. Ngai, R. Casalini, and C. M. Roland, Macromolecules **38**, 4363 (2005).
[49] K. Adachi and H. Hirano, Macromolecules **31**, 3958 (1998).
[50] P. G. Santangelo and C. M. Roland, Macromolecules **31**, 3715 (1998).
[51] T. Nicolai and G. Floudas, Macromolecules **31**, 2578 (1998).
[52] C. M. Roland, K. L. Ngai, P. G. Santangelo, XH. Qiu, M. D. Ediger, and D. J. Plazek, Macromolecules **34**, 6159 (2001).